EC
Journals.ASM.org

Role of Fig1, a Component of the Low-Affinity Calcium Uptake System, in Growth and Sexual Development of Filamentous Fungi

Brad Cavinder[a] and Frances Trail[b,c]

Genetics Graduate Program,[a] Department of Plant Biology,[b] and Department of Plant Pathology,[c] Michigan State University, East Lansing, Michigan, USA

The function of Fig1, a transmembrane protein of the low-affinity calcium uptake system (LACS) in fungi, was examined for its role in the growth and development of the plant pathogen *Fusarium graminearum*. The Δ*fig1* mutants failed to produce mature perithecia, and sexual development was halted prior to the formation of perithecium initials. The loss of Fig1 function also resulted in a reduced vegetative growth rate. Macroconidium production was reduced 70-fold in the Δ*fig1* mutants compared to the wild type. The function of the high-affinity calcium uptake system (HACS), comprised of the Ca^{2+} channels Mid1 and Cch1, was previously characterized for *F. graminearum*. To better understand the roles of the LACS and the HACS, Δ*fig1* Δ*mid1*, Δ*fig1* Δ*cch1*, and Δ*fig1* Δ*mid1* Δ*cch1* double and triple mutants were generated, and the phenotypes of these mutants were more severe than those of the Δ*fig1* mutants. Pathogenicity on wheat was unaffected for the Δ*fig1* mutants, but the Δ*fig1* Δ*mid1*, Δ*fig1* Δ*cch1*, and Δ*fig1* Δ*mid1* Δ*cch1* mutants, lacking both LACS and HACS functions, had reduced pathogenicity. Additionally, Δ*fig1* mutants of *Neurospora crassa* were examined and did not affect filamentous growth or female fertility in a Δ*fig1* mating type *A* strain, but the Δ*fig1* mating type *a* strain failed to produce fertile fruiting bodies. These results are the first report of Fig1 function in filamentous ascomycetes and expand its role to include complex fruiting body and ascus development.

Calcium is a ubiquitous messenger in eukaryotic cells, acting both directly and indirectly to modulate protein activity, gene transcription, energy metabolism, endo- and exocytosis, and many other cellular processes (4, 13, 48). In fungi, two major calcium uptake pathways have been identified and characterized: the high-affinity calcium uptake system (HACS), active during low calcium availability, and the low-affinity calcium uptake system (LACS), active when calcium availability is high (24, 27, 38, 45, 50). A third calcium uptake pathway was recently described for *Saccharomyces cerevisiae* but has yet to have its genetic components identified (34). In the filamentous fungus *Fusarium graminearum* (sexual-stage *Gibberella zeae*), the causal agent of head blight of wheat and barley, calcium signaling has been shown to have a role in hyphal growth, sporulation, and fruiting body function, and the regulation of components of the HACS has been shown to be involved in these processes (17, 35, 62, 63).

The HACS is minimally composed of the voltage-gated Ca^{2+} channel (VGCC) Cch1 (27, 50), the stretch-activated calcium channel/regulatory protein Mid1 (38), and the PMP22_Claudin superfamily member regulatory protein Ecm7 (45). In yeasts, the HACS responds to environmental and endoplasmic reticulum stress and to exposure to mating pheromone (8, 9, 20, 36, 38, 42, 51, 65). In filamentous fungi, HACS mutants show both shared and variable phenotypes across species, including reduced vegetative growth and calcium homeostasis lesions for most species and effects on pathogenicity and sexual development for some species (6, 17, 35, 40).

The LACS is minimally composed of the Fig1 membrane protein, a PMP22_Claudin superfamily member, like Ecm7, and is involved in calcium influx and membrane fusion during the mating of *S. cerevisiae* and *Candida albicans* (49, 69), mating projection development and cell wall degradation at the fusion site of appressed shmoos in *S. cerevisiae* (24), and thigmotropism and the repression of hyphal growth in *C. albicans* (9). Mammalian PMP22_Claudin superfamily members are involved in membrane-membrane interactions such as epithelial tight-junction formation and signal transduction such as ion flux (46, 64). The fungal members show little overall sequence identity with their mammalian orthologs, but most have similar secondary structures and topologies, including cytoplasmic N and C termini, four transmembrane domains, two extracellular loops and one intracellular loop, and a conserved GΦΦGXC(n)C motif (where Φ is F, L, M, or Y hydrophobic residues; $8 < n < 20$ amino acids [aa]) in the first extracellular loop (9, 24, 73).

In *F. graminearum*, the deletion of *CCH1*, *MID1*, or both resulted in almost identical phenotypes, including a reduced vegetative growth rate, conidiation, ascospore development, and forcible ascospore discharge from asci. Chemical complementation with exogenous calcium rescued all phenotypes, at least partially, except for the abnormal ascospore development seen in strains lacking Mid1, including the Δ*cch1* Δ*mid1* double mutant (17, 35). Because the addition of calcium rescued most phenotypes, including those of the Δ*cch1* Δ*mid1* double mutant, and because the LACS is involved in calcium importation, is active in environments with a high calcium availability, and is involved in the sexual development of yeasts, we investigated the role of Fig1 in the growth and development of *F. graminearum*. We asked whether Fig1 is involved in the uptake of calcium, which is essential for the chemical complementation of the HACS mutant phenotype. We identified the putative *F. graminearum FIG1* ortholog and generated Δ*fig1*, Δ*cch1* Δ*fig1*, Δ*fig1* Δ*mid1*, and Δ*cch1* Δ*fig1* Δ*mid1* strains to characterize the Fig1 function and interactions with HACS components. Additionally, we investigated the effect of the loss of Fig1 on growth, calcium homeostasis, and sexual develop-

Received 5 January 2012 **Accepted** 16 May 2012
Published ahead of print 25 May 2012
Address correspondence to Frances Trail, trail@msu.edu.
Supplemental material for this article may be found at http://ec.asm.org/.

doi:10.1128/EC.00007-12

TABLE 1 Strains used in this study

Strain	Genotype	Abbreviation	Reference
Fusarium graminearum			
PH-1(FGSC 9075)	Wild type (NRRL 31084)	wt	61
PH-1 55	*nit3*		17
Δfig1-1	Δ*fig1*	Δf1	This study
Δfig1-2	Δ*fig1*	Δf2	This study
Δ*cch1*-T11	Δ*cch1*		35
mn-11	Δ*mid1 nit3*		17
cn-5	Δ*cch1 nit3*		This study
cn-7	Δ*cch1 nit3*		This study
cmn-1	Δ*cch1* Δ*mid1 nit3*		This study
cmn-9	Δ*cch1* Δ*mid1 nit3*		This study
fm-1	Δ*fig1* Δ*mid1*		This study
fm-5	Δ*fig1* Δ*mid1*	ΔfΔm	This study
fc-1	Δ*fig1* Δ*cch1*		This study
fc-6	Δ*fig1* Δ*cch1*	ΔfΔc	This study
fcm-2	Δ*mid1* Δ*cch1* Δ*fig1*	ΔfΔcΔm	This study
f12-C1	Δ*fig1*::*FIG1*	Δf12-C1	This study
f12-C2	Δ*fig1*::*FIG1*	Δf12-C2	This study
Neurospora crassa			
FGSC_2489	Wild type, *A*	wt *A*	19[a]
FGSC_4200	Wild type, *a*	wt *a*	19[a]
FGSC_17273	Δ*fig1*, *a*	*fig1 a*	19[a]
fig1a-22	Δ*fig1*, *a*		This study
fig1a-23	Δ*fig1*, *A*		This study
fig1A-18	Δ*fig1*, *A*	*fig1 A*	This study
fig1A-20	Δ*fig1*, *A*		This study
fig1A-21	Δ*fig1*, *A*		This study

[a] Received directly from the Fungal Genetics Stock Center.

ment in *Neurospora crassa*, which has been shown to have different roles for HACS components than *F. graminearum* (17, 40).

MATERIALS AND METHODS

Strains and culture conditions. Strains used in this study are described in Table 1. Strains of *F. graminearum* were maintained on sterile soil at −20°C, as macroconidia (10^6 to 10^8 conidia/ml), and as colonized pieces of V8 agar in sterile 35% glycerol at −80°C. Macroconidia were produced in carboxymethylcellulose (CMC) liquid medium, as previously described (12), or on Bilay's agar medium (5). Sexual development was induced in cultures on carrot agar by the gentle removal of surface mycelia, followed by treatment with 1 ml of a 2.5% (wt/vol) Tween 60 solution, as previously detailed (7, 61). Although *F. graminearum* is homothallic, it can outcross, a process accomplished by inoculating carrot agar with two different strains side by side. Recombinant perithecia are found along the centerline where the colonies meet.

N. crassa is heterothallic, with two mating type idiomorphs, *a* and *A* (30, 47). *N. crassa* wild-type (wt) and Δ*fig1* mating type *a* (19) strains were obtained from the Fungal Genetics Stock Center (FGSC) and were maintained on synthetic crossing (SC) medium (22) slants at −20°C. Sexual crosses were performed as previously described, except that cultures on SC medium were incubated for 7 days in ambient light instead of continuous fluorescent lighting (17).

Nucleic acid manipulation and genetic transformation. DNA was extracted from *F. graminearum* and *N. crassa* mycelia by using a hexadecyltrimethylammonium bromide (CTAB)-based method, as previously described (17). *F. graminearum* and *N. crassa* nucleotide data were obtained from the Munich Information Center for Protein Sequences (MIPS) *Fusarium graminearum* Genome Database (version 3.2; http://mips.helmholtz-muenchen.de/genre/proj/FGDB/) and the MIPS *Neurospora crassa* Genome Database (http://mips.helmholtz-muenchen.de/genre/proj/ncrassa/ [accessed June 2011]), respectively. Primers used in this study are listed in Table S1 in the supplemental material. Phusion high-fidelity DNA polymerase (New England BioLabs, Ipswich, MA) was used for PCR unless otherwise noted. For targeted gene replacement constructs, a split-marker protocol (14, 25, 26) was performed as previously described (17), with modifications to target *Fig1* with the hygromycin resistance (*hph*) marker from pCB1004 (13), as described below.

The split-marker technique involves the amplification of 500- to 750-bp fragments immediately upstream (L) and downstream (R) of the coding sequence of the target gene with 3′ and 5′ tails complementary to the 5′ and 3′ ends of the *hph* marker, respectively, allowing the fusion of the L and R flanks to overlapping partial *hph* amplicons by PCR. A successful gene replacement will result from a crossover between the *hph* fragments of the two merged products and the replacement of the *Fig1* gene with the crossover fragment. In the case of *FIG1*, the annotated stop codon was 36 bp upstream from a contig gap, so we used 473 bp of coding sequence upstream of the contig gap to generate the R fragment. Therefore, the final construct resulted in a partial gene replacement rather than a full gene replacement, with 475 nucleotides of the reference gene sequence remaining in the genome of the replacement strains. For the generation of the Δ*fig1* single mutants, the L-*hph* fragment (593 bp; supercontig_3.3, positions 4947747 to 4947176) was amplified by primers Fig1-L5 and Fig1-L3-Hyg, while primers Fig1-R5-Hyg and Fig1-R3 generated a 474-bp R-*hph* fragment (supercontig_3.3, positions 4947302 to 4947775). Primers Fig1-L3-Hyg and Fig1-R5-Hyg had 5′ tails of 15 and 20 bases complementary to the 5′ and 3′ ends of the *hph* marker from pCB1004 (13), respectively, allowing for the selection of transformants with hygromycin B (HygB). For split *hph*, Fig1-HygF and Fig1-HygR contained 5′ tails of 13 and 15 bases complementary to the 3′ and 5′ ends of the *FIG1* sequences of the Fig1 L- and R-*hph* fragments and were paired with primers 5′ 1/2 HygR and 3′ 1/2 HygF to generate the 5′ and 3′ *hph* fragments, respectively. The 5′ *hph* and L-*hph* and the 3′ *hph* and R-*hph* fragments were merged together by using PCR. Both merged products were transformed into wt *F. graminearum* protoplasts.

For the complementation of the Δ*fig1* mutants, a 1,599-bp fragment of the *FIG1* locus (FGSG_06302; supercontig_3.3, positions 4946177 to 4947775), spanning 1,000 bp upstream of the first (supercontig_3.3, position 4947177) and to 2 bp upstream of the last (supercontig_3.3, position 4947777) *FIG1* coding nucleotides, was generated by PCR using primers Fig1-compF and Fig1-compR. The amplicon was used to transform Δ*fig1* protoplasts.

The polyethylene glycol-mediated transformation of protoplasts of *F. graminearum* was performed after 15 h of growth; the transformed protoplasts were overlaid with medium containing 200 μg/ml HygB for selection, as previously described (29). Colonies that grew through to the surface of the overlay were transferred onto V8 agar containing 450 μg/ml HygB. For the complementation of Δ*fig1* mutants, the selection of transformants was done by using the calcium ionophore A23187. Because A23187 had not been used previously for selection, the complementation reaction mixture was divided into three groups and overlaid with regeneration medium containing either 0.57 mM, 1.4 mM, or 3.1 mM ionophore A23187. Colonies that emerged on the surface of the overlays were transferred onto V8 agar amended with 2 mM A23187. Transformants thriving on selective medium were then transferred onto V8 agar for maintenance, storage, and subsequent phenotype analysis.

RNA was extracted from lyophilized *F. graminearum* mycelia by using TRIzol reagent (Life Technologies, Carlsbad, CA) according to the manufacturer's protocol, with two phenol (pH 6.6)-chloroform-isoamyl alcohol (25:24:1) extraction steps followed by two chloroform extraction steps after the initial TRIzol-chloroform phase separation. Sample aliquots of 120 μg were purified by using the RNeasy minikit (Qiagen, Germantown, MD) according to the manufacturer's RNA cleanup instructions and by elution with nuclease-free H_2O (Promega). All RNA was stored at −80°C.

One microgram of RNA was used as the template for cDNA synthesis reactions. The SMARTer RACE cDNA amplification kit (Clontech, Mountain View, CA) was used for cDNA synthesis for subsequent 5′ rapid amplification of cDNA ends (5′-RACE) and 3′-RACE reactions according to the manufacturer's instructions. Along with the universal primer in-

cluded in the kit, primers Fig1 RACE R1 and Fig1 RACE F1 for the 5′- and 3′-RACE reactions, respectively, and Phusion high-fidelity DNA polymerase (NEB) were used in the RACE reaction mixtures. Amplified fragments were then cloned into pCR2.1-TOPO by using the TOPO TA cloning kit (Life Technologies) and sequenced at Michigan State University's Research Technology Support Facility by using an ABI Prism 3730 genetic analyzer (Life Technologies). Reverse transcription (RT)-PCR to detect *FIG1* expression was performed by using primers Fig1 RT-F and Fig1 RT-R, which span the splice junctions between exons 1 and 2 and exons 3 and 4, with the 3′ ends consisting of 6 bp of exon 2 and exon 3, respectively. The expression of the gene for elongation factor 1A (*EF1A*) (FGSG_08811) was detected by using primers EF1A-F and EF1A-R, which do not span exon splice junctions.

Analysis of sexual crosses. All *F. graminearum* crosses were performed between *NIT3* (FGSG_10250) (probable nitrilase) nitrate-utilizing (nit^+) and *nit3* non-nitrate-utilizing mutant (nit^-) strains. Cirrhi (spores oozing from perithecia) from single perithecia were collected individually, and the spores were suspended in water and distributed across the surface of MMTS medium, as previously described (7, 17). Recombinant perithecia can easily be identified by the presence of approximately equal numbers of nit^+ and nit^- progeny, which have different growth phenotypes on this medium. For strains that did not form cirrhi (*cch1* and *mid1* mutants), 10 perithecia at the interface between strains were collected, crushed in bulk on a glass slide in sterile distilled H_2O to release ascospores, and rinsed off the glass slides, and a portion of the suspension was spread onto the surface of MMTS agar. After 5 to 7 days of growth at room temperature, nit^+ and nit^- colonies from recombinant perithecia or bulk mixtures were individually collected. To confirm the nit phenotype, cultures were subsequently transferred onto Czapek-Dox agar (60) and Czapek-Dox agar supplemented with 470 mM potassium chlorate and 0.17% L-arginine (68). PCR was used to confirm the presence or absence of *CCH1*, *FIG1*, and *MID1*.

To generate *N. crassa* Δ*fig1* mating type *A* mutants, a Δ*fig1* mating type *a* mutant strain (FGSG_17273) was crossed with a wt mating type *A* strain (FGSG_4200). To recover progeny, ascospores were then rinsed off the lids, subjected to heat shock to promote germination, and placed onto SC medium amended with 1% sorbose and 0.05% glucose and fructose, with sucrose omitted for germination, as previously described (52, 58, 59). Single-spore isolates were transferred into SC medium, and PCR was used to confirm the presence or absence of *fig1* and mating type *A*-2 (present in mating type *A* and absent in mating type *a*).

Characterization of Δ*fig1* phenotypes. To characterize the vegetative growth and sexual development of *F. graminearum* Δ*fig1* strains, individual strains were grown on carrot agar amended with 80 mM $CaCl_2$ or 80 mM $MgCl_2$ or unamended and incubated at room temperature under continuous light. Radial growth was measured at 24-h intervals for 3 days, with four biological replicates for each strain. The first day's growth was discounted. The growth rate was calculated by subtracting the colony diameter at 24 h from the diameter at 48 h and was averaged between the replicates. Significance between the growth of Δ*fig1* strains compared to the growth of wt and among the treatments was assessed. Bilay's medium (5) was supplemented to 1 mM with the extracellular calcium chelator 1,2-bis(2-aminophenoxy)ethane-*N*,*N*,*N*,*N*-tetraacetic acid tetrapotassium salt (BAPTA) to determine the ability of Δ*fig1* mutants to grow under conditions of limited calcium, as previously described for Δ*cch1* mutants (17). To determine the effect of increased intracellular calcium levels, strains were center inoculated onto V8 agar, and after 48 h of growth, a point treatment of 10 μl of either a 9.5 mM solution of the calcium ionophore A23187 (in ethyl alcohol [EtOH]) or 100% EtOH (control) was applied onto a point slightly ahead of the leading edge of the mycelial growth.

To quantify conidiation in *F. graminearum* mutants, strains were grown with shaking in 100 ml CMC for 4 days at room temperature. Macroconidia were harvested by filtration through sterilized Miracloth (Calbiochem). The macroconidia were pelleted by centrifugation, resuspended in 1 ml of sterile distilled H_2O, and quantified.

PCR-identified Δ*fig1* mating type *A* progeny of *N. crassa* were reciprocally crossed to wt mating type *a*, wt mating type *A*, and Δ*fig1* mating type *A* strains both to test the mating type determination and to assess the effect of the loss of Fig1 on sexual development. Squash mounts of perithecia from the crosses were examined microscopically to observe ascus and ascospore development. Culture dish lids of the crosses were monitored for discharged ascospores. For the quantification of macroconidia, cultures were grown on synthetic crossing medium in plates sealed with Parafilm. After 3 days of growth, the Parafilm was removed, and the cultures were allowed to sporulate for 3 days. Spores were suspended in water with Tween 60 and quantified. Three trials were performed for each strain.

Pathogenicity assays were performed, as previously described (35), by the inoculation of a central floret of spring wheat cultivar Wheaten with 10 μl of the conidial stock of the appropriate strain. Ten wheat heads at anthesis were inoculated with each strain. Following 72 h in a misting chamber, symptoms were monitored for up to 2 weeks. The experiment was repeated twice.

Statistical analysis. To assess the significance of intragroup variations and intergroup interactions and to return associated *P* values for all pairwise comparisons, an analysis of variance (ANOVA) and Tukey's honestly significant difference (HSD) test were performed using by the R language and environment for Windows (53).

Illumina sequencing and bioinformatics. Genomic DNA from an insertional mutant generated from wt strain PH-1 was sequenced by using Illumina GAII (San Diego, CA) with 76-bp paired-end reads and a 400-bp average library insert size. The 3′ ends of the reads were trimmed with a Biopython script (18) and a Phred scale quality cutoff score of 28. The reads were assembled by using the Velvet assembler (version 1.1.03), using k-mer values of 37 to 49 nucleotides (71, 72). No reads were manually discarded because of length, but reads shorter than the k-mer size used in an assembly are automatically ignored by Velvet. The *FIG1* locus was located in the assembly by using standalone BLAST+ (11). A sequencing library was constructed from wt RNA collected from perithecia at 96 h after the induction of sexual development and sequenced by using Illumina GAII 36-bp single-end reads and a 400-bp average cDNA library insert size (58a).

Burrows-Wheeler Aligner (BWA) (version 0.5.9) (41) was used to align the RNAseq reads to either the genomic *FIG1* sequence from the Velvet assembly or the same sequence with the introns removed. The 5′- and 3′-RACE clone sequences were aligned manually. A multiple-sequence alignment of the sequence of the putative full-length *F. graminearum* Fig1 protein to Fig1 sequences from multiple fungi was performed with T-Coffee (23). The multiple-sequence alignment was viewed and edited with Jalview (66) and Seaview (32). The putative full-length *F. graminearum* Fig1 protein sequence was used to search the Conserved Domains Database (44).

Microscopy and imaging. For microscopic examination, samples were fixed in 2× phosphate-buffered saline (PBS) containing 4% (wt/vol) paraformaldehyde for 20 min on ice, washed twice with 2× PBS, and stained with 0.06% (wt/vol) toluidine blue in sterile H_2O overnight. Stained samples were washed twice each in 50%, 75%, and 100% ethanol in sterile water before being stored in sterile H_2O. To determine whether sexual development initiates at all or if it halts at a very early stage of development, the wt and the Δ*fig1* single mutants were inoculated onto carrot agar with several pieces of a cellulose membrane placed onto the surface of the medium. At 24 h and 48 h postinduction, the cellulose membranes were removed from the carrot agar, and the membranes were fixed, stained with toluidine blue, destained, and viewed by light microscopy.

A Zeiss (Göttingen, Germany) standard microscope was used to observe samples, and images were captured with a Zeiss AxioCam MRc color camera by using AxioVision 4.8.2. Nonmicroscopic images were captured with a Nikon (Tokyo, Japan) Coolpix 995 camera. Image processing and

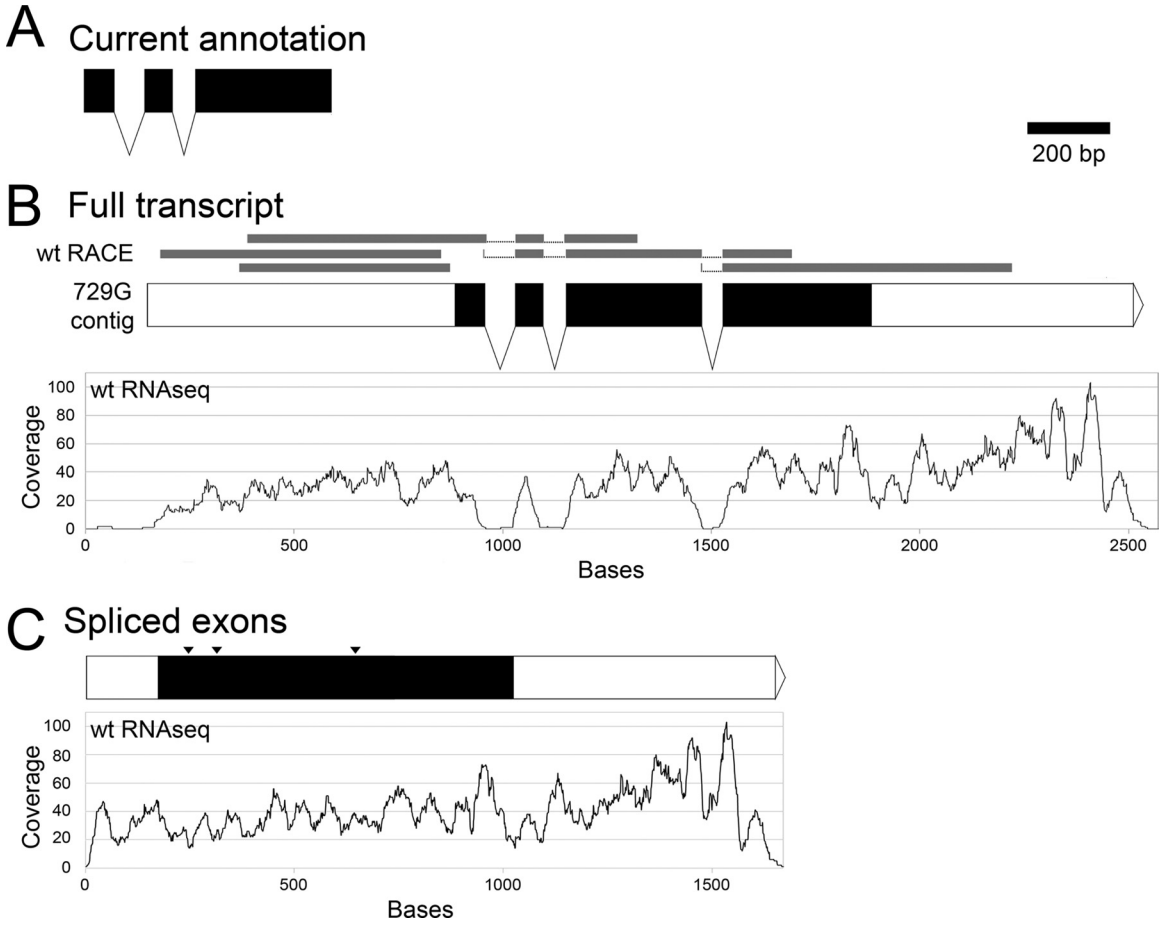

FIG 1 *F. graminearum FIG1* gene models. (A) Current gene model from MIPS. (B) Predicted gene model from a Velvet assembly of insertion mutant 729g-112. Gray bars above the model represent aligned 5′- and 3′-RACE clone sequences. The graph below the model shows the coverage of aligned wt RNAseq reads. (C) Predicted spliced transcript from wt RACE and RNAseq alignments in panel B. Only a portion of the 5′-untranslated region is shown; the locations of splice sites are indicated (arrowheads). An alignment of the wt RNAseq reads to the model sequence is graphed below the model. Scale bar, 200 bp.

annotation were performed with ImageJ (1) or Adobe (San Jose, CA) Photoshop CS2.

Nucleotide sequence accession number. The GenBank accession number for the *F. graminearum* Fig1 protein is JX003250.

RESULTS

Identification of *FIG1* through RACE and Illumina sequencing. The reference sequence of *F. graminearum* contained a contig gap in the region of *FIG1* (assembly 3, contigs 204 and 205) (*Fusarium* Comparative Sequencing Project, Broad Institute of Harvard and MIT [http://www.broadinstitute.org/annotation/genome/fusarium_graminearum/MultiHome.html]). Due to the gap, the *FIG1* annotation (in both the MIPS *Fusarium graminearum* Genome Database and the Broad Institute *Fusarium* Comparative Database) contained two introns and three exons (Fig. 1A) ending 36 bp upstream of the contig gap, predicting a protein of 156 amino acids that is more than 100 aa shorter than most filamentous ascomycete homologs. To recover the missing sequence, 5′- and 3′-RACE were performed, and two clones from each preparation were sequenced, revealing the presence of a third intron and a fourth exon (Fig. 1B). Subsequently, we performed Illumina sequencing on genomic DNA from a strain derived from the wt (data not shown). In addition, Illumina RNAseq was performed on developmental stages of the wt (58a). The *FIG1* genomic sequence was identified from the Velvet assembly of the genomic DNA by BLAST. The sequence spanning the annotated end of the previous gene upstream to the start of the next gene downstream of *FIG1* was used for the alignment. The RACE sequences and RNAseq reads were aligned to the Velvet *FIG1* sequence, and both sets of data aligned well to the exons but not the introns (Fig. 1B). The introns were removed from the Velvet *FIG1* genomic sequence, and the RNAseq reads were aligned to the putative spliced transcript, resulting in read coverage across the splice junctions instead of the loss of coverage seen with the introns included (Fig. 1C).

RNAseq data were also used to examine gene expression levels across vegetative growth and development. RPKM (reads aligned per kilobases mapped) values for *MID1*, *CCH1*, and *MID1* are presented in Table S3 in the supplemental material. These values indicate that *MID1* and *CCH1* were expressed constitutively, but *FIG1* showed the highest expression levels during vegetative growth, the lowest expression levels at 24 h after the induction of sexual development, and increased expression levels throughout the maturation of the asci (72 h to 144 h).

To assess whether the *F. graminearum FIG1* sequence from the

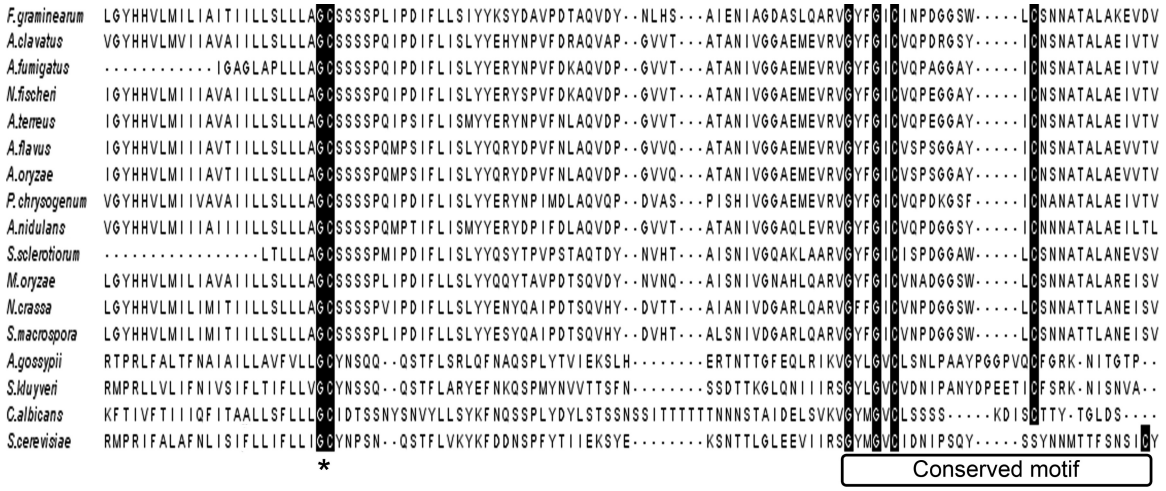

FIG 2 Multiple-amino-acid sequence alignment of a region of Fig1 homologs. Highly conserved glycine and cysteine residues of a conserved Gly-Cys motif, at or near the end of the first transmembrane domain of the proteins (*), and a conserved claudin motif are highlighted with a black background. *A. clavatus*, *Aspergillus clavatus*; *N. fischeri*, *Neosartorya fischeri*; *A. terreus*, *Aspergillus terreus*; *A. flavus*, *Aspergillus flavus*; *A. oryzae*, *Aspergillus oryzae*; *P. chrysogenum*, *Penicillium chrysogenum*; *S. sclerotiorum*, *Sclerotina sclerotiorum*; *M. oryzae*, *Magnaporthe oryzae*; *A. gossypii*, *Ashbya gossypii*; *S. kluyveri*, *Saccharomyces kluyveri*.

Velvet assembly represented the full length of the gene, the translated protein sequence was aligned to 16 Fig1 homologs from ascomycetes (see Table S2 in the supplemental material). The Claudin motif is present in all Fig1 homologs (Fig. 2). The longer protein aligned well across the full length of the protein, especially to other filamentous species (data not shown), and a search of the Conserved Domains Database (44) found a full-length Fig1 domain (data not shown), indicating that the longer sequence included the complete *F. graminearum FIG1* ortholog.

Generation and characterization of *FIG1* mutants of *F. graminearum*. *F. graminearum FIG1* mutants were generated by replacing the first 125 bp of the coding sequence with *hph*. From a single transformation experiment, 10 transformants resistant to hygromycin were obtained. PCR amplicons of three transformants were consistent with the replacement of the targeted *FIG1* sequence with *hph*, and the remaining 7 transformants were not tested (not shown). Two of these three transformants, designated Δfig1-1 and Δfig1-2, were used in subsequent experiments. RT-PCR detected *FIG1* expression in wt cDNA but not wt genomic DNA or Δfig1-1 and Δfig1-2 cDNAs (see Fig. S1 in the supplemental material). Δfig1-2 protoplasts were used to recover complemented transformants following selection with the calcium ionophore A23187. From equal numbers of protoplasts, two were recovered from selection with 3.1 mM ionophore, more than 70 were recovered using 1.4 mM ionophore for selection, and none were recovered using 0.57 mM ionophore for selection. PCR amplicons of the two transformants isolated using 3.1 mM A23187 were consistent with an integration of the complementing DNA fragment, while amplicons for the four putative transformants from the plates containing 1.4 mM A23187 indicated that they were still Δ*fig1*.

To generate Δ*cch1 nit3* and Δ*cch1* Δ*mid1 nit3* strains, crosses were initiated between Δ*cch1*-T11 (Δ*cch1*) and mn-11 (Δ*mid1 nit3*). PCR screening of 12 progeny growing slowly and sparsely on MMTS agar (indicative of a nit$^-$ phenotype) revealed two strains, cn-5 and cn-7, that produced the amplicons expected from a Δ*cch1* genotype and two strains, cmn-1 and cmn-9, that produced the amplicons expected from a Δ*cch1* Δ*mid1* genotype. Crosses of Δfig1-1 × mn-11, Δfig1-1 × cn-7 (Δ*cch1 nit3*), and Δfig1-1 × cmn-1 (Δ*cch1* Δ*mid1 nit3*) were performed to isolate Δ*fig1* Δ*mid1*, Δ*cch1* Δ*fig1*, and Δ*cch1* Δ*fig1* Δ*mid1* strains, respectively. Six progeny displaying slow and dense growth on MMTS agar (indicative of a nit$^+$ phenotype) were recovered from each of the three crosses. Screening by PCR confirmed the presence of the appropriate amplicons for two Δ*fig1* Δ*mid1* strains (fm-1 and fm-5), two Δ*cch1* Δ*fig1* strains (fc-1 and fc-6), and one Δ*cch1* Δ*fig1* Δ*mid1* strain (fcm-2).

To examine the effects of the *FIG1* deletion on vegetative growth, calcium uptake, and calcium homeostasis, all strains were grown on medium with or without the addition of calcium, magnesium, the calcium chelator BAPTA, and the calcium ionophore A23187 (which increases the cytosolic concentration of calcium). Differences in mycelial growth were tested under several conditions. Growth on unamended carrot agar revealed that all LACS and HACS mutants grew at a lower rate than the wt (Fig. 3A). Growth on Bilay's medium containing 1 mM BAPTA was used to test growth in calcium-restrictive medium. As previously reported, strains lacking Mid1 or Cch1 grew slightly for 1 day and failed to colonize the BAPTA medium further (17, 35), but Δ*fig1* mutants fully colonized the medium, as did the wt. Growth on V8 agar spot amended with either the calcium ionophore A23187 or EtOH (control) showed that the wt fully colonized the A23187-treated medium, while the other strains were unable to colonize the treated spot (Fig. 3B). Previous work showed that strains lacking Cch1 or Mid1 were also unable to colonize the A23187-treated spot (17). All strains colonized the EtOH control medium, and the phenotypes of complemented strains F12-C1 and F12-C2 (not shown) were similar to that of the wt.

A quantification of growth rates and macroconidium production was performed to better understand the effect of the loss of Fig1 on vegetative growth and asexual reproduction. When grown on unamended carrot agar, Δ*fig1* mutants grew at a significantly lower rate than the wt, while mutants having both LACS and HACS defects grew at a significantly lower rate than the Δ*fig1*

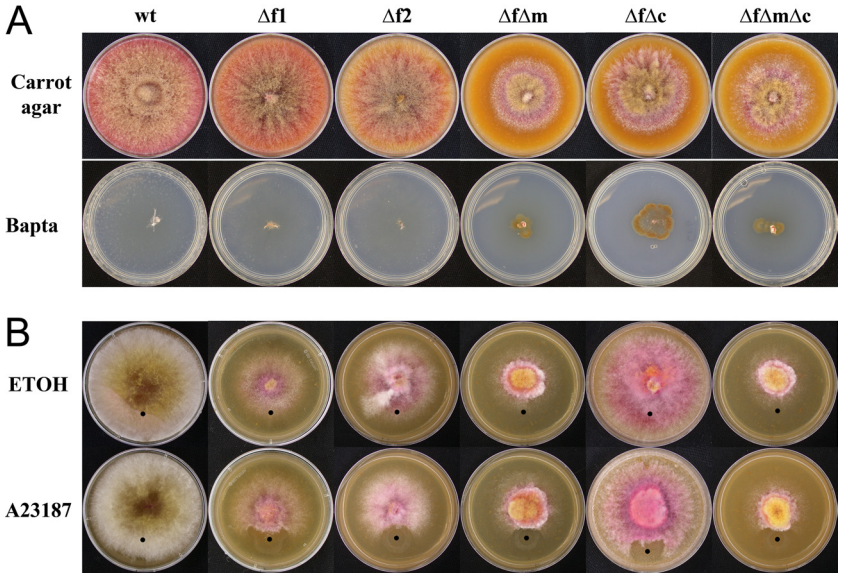

FIG 3 Vegetative growth of *F. graminearum* strains. (A, top) Growth on carrot agar. While the wt, Δfig1-1, and Δfig1-2 fully colonized the surface of the medium in 4 days, the growth rates of strains fm-5, fc-6, and fcm-2 were reduced. (Bottom) Growth (14 days) on carrot agar supplemented with1 mM BAPTA. The wt, Δfig1-1, and Δfig1-2 fully colonized the surface of the medium, but strains fm-5, fc-6, and fcm-2 ceased growth after some initial colonization. (B, top) Growth on V8 agar with EtOH (control). While the wt fully colonized the surface of the medium in 4 days, strains Δfig1-1 and Δfig1-2 had reduced growth and fewer aerial hyphae than the wt. Strains fm-5, fc-6, and fcm-2 had more severe phenotypes than did strains with single mutations. (Bottom) Growth on V8 in the presence of the Ca^{2+} ionophore A23187 (the application point is indicated by a black dot). The wt fully colonized the ionophore-treated medium (lower portion of the colonies), but in all mutant strains, the presence of the ionophore halted growth. Strains and genotypes are abbreviated as follows: wt (*FIG1 MID1 CCH1*); Δf1, Δfig1-1 (Δ*fig1 MID1 CCH1*); Δf2, Δfig1-2 (Δ*fig1 MID1 CCH1*); ΔfΔm, fm-5 (Δ*fig1* Δ*mid1 CCH1*); ΔfΔc, fc-6 (Δ*fig1 MID1* Δ*cch1*); ΔfΔmΔc, fcm-2 (Δ*fig1* Δ*mid1* Δ*cch1*).

strains. The growth rates of complemented strains f12-C1 and f12-C2 were not significantly different from that of the wt (Fig. 4A). The Δ*fig1* Δ*mid1* and Δ*fig1* Δ*cch1* results were nearly the same as those previously reported for single Δ*mid1* and Δ*cch1* mutants (17, 35). The growth of strains on carrot agar amended with 80 mM calcium or 80 mM magnesium was not significantly different from the growth of the same strain on unamended carrot agar, except for the Δ*cch1* Δ*fig1* Δ*mid1* triple mutant, which grew significantly more slowly on carrot agar amended with magnesium than on both carrot agar and carrot agar amended with calcium. These results differed from previously obtained results for Δ*mid1*, Δ*cch1*, and Δ*mid1* Δ*cch1* mutants in that these mutants all showed significant increases in growth rates upon exogenous calcium treatment (17, 35). Additionally, the Δ*mid1* Δ*cch1* mutant did not have a decreased growth rate upon the addition of exogenous magnesium (17). All mutants produced significantly fewer macroconidia in CMC medium than the wt but were not significantly different from each other (Fig. 4B). The Δ*fig1* mutant conidiation phenotype was slightly more severe than that previously reported for Δ*mid1* mutants, and the numbers of conidia produced by the Δ*fig1* Δ*mid1*, Δ*mid1* Δ*cch1*, and Δ*fig1* Δ*mid1* Δ*cch1* mutants were an order of magnitude lower than those produced by the Δ*mid1* and Δ*mid1* Δ*cch1* mutants (17).

All strains lacking functional Fig1 failed to develop perithecia, including the double and triple mutants with the HACS components Mid1 and Cch1, although they produced the characteristic black pigment seen in the top 2 to 4 mm of the medium after induction (Fig. 5A). Previously reported results for Δ*mid1*, Δ*cch1*, and Δ*mid1* Δ*cch1* mutants showed slowed sexual development, reduced ascospore discharge, and some abnormally developed ascospores (17, 35). To determine whether sexual development initiates at all or if it halts at a very early stage of development, the wt and the Δ*fig1* single mutants were inoculated onto carrot agar with several pieces of cellulose membrane placed onto the surface of the medium. At 24 h, the wt developed perithecium initials, but the Δ*fig1* mutants had only small hyphae curving back onto themselves. By 48 h, the membranes with the wt contained larger immature perithecia with developing walls, and the curved hyphae of the Δ*fig1* mutant enlarged but failed to develop any further (Fig. 5B).

Pathogenicity assays showed that wheat inoculated with the Δ*fig1* and Δ*fig2* strains developed symptoms similar to those of the wt (all 10 heads developed symptoms), although full symptoms were delayed by 1 week in comparison to the wt. The Δ*fig1* Δ*mid1* and Δ*fig1* Δ*cch1* strains showed similar delays in symptom development and reduced pathogenicity, with fewer than 5 of the 10 inoculated heads developing symptoms with each strain in both experiments. The Δ*fig1* Δ*mid1* Δ*cch1* triple mutant failed to develop symptoms in any of the heads inoculated.

Characterization of *N. crassa fig1* mutants. The *N. crassa fig1* ortholog (NCU02219) was identified by BLAST using the *S. cerevisiae* Fig1 protein sequence. A Δ*fig1* mating type *a* strain, but not a Δ*fig1* mating type *A* strain, was generated previously by Colot et al. (19), so the Δ*fig1* mating type *a* strain was crossed to a wt mating type *A* strain to generate Δ*fig1* mating type *A* progeny. Twenty-four progeny were screened by PCR for the absence of *fig1* and the presence of the mating type *A*-2 gene. PCR analysis revealed that three progeny, fig1A-18, fig1A-20, and fig1A-21, lacked *fig1* but harbored the mating type *A*-2 gene. Strain fig1A-21 was used for

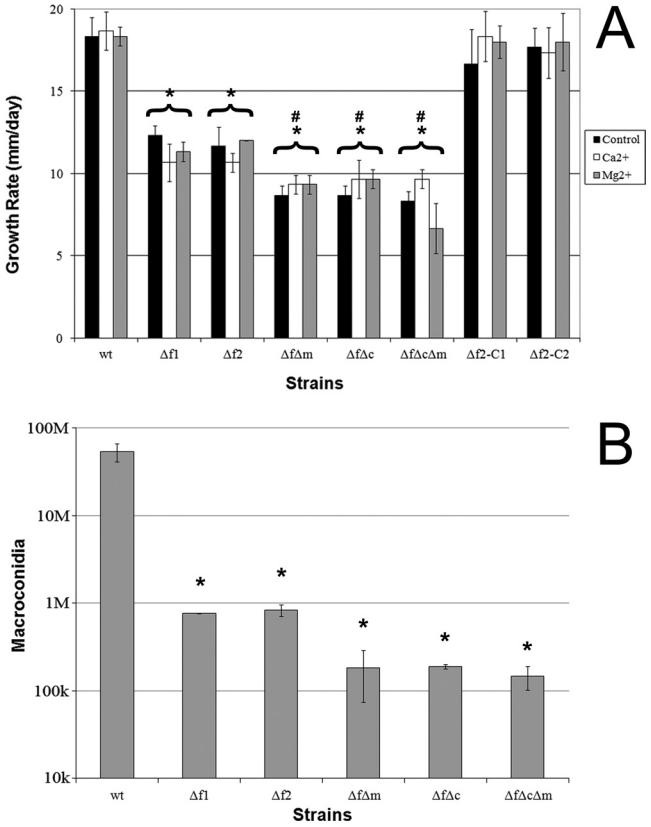

FIG 4 Characterization of *F. graminearum* growth and asexual development. (A) Growth rates on carrot agar with and without Ca^{2+} or Mg^{2+} supplementation (change of diameter in mm/day). Asterisks above brackets indicate a significant difference between all growth conditions of the bracketed strain and the wild type on carrot agar. Number signs above brackets indicate a significant difference between the bracketed strain on carrot agar and strain Δfig1-1, but not Δfig1-2, on carrot agar. (B) Macroconidium production. Error bars represent the standard deviations of the means from 3 biological replicates. *, $P < 0.005$; #, $P < 0.05$. Abbreviations for strains and genotypes are listed in the legend of Fig. 3, except that Δf2-C1 indicates f12-C1 (Δ*fig1*::*FIG1 MID1 CCH1*) and Δf2-C2 indicates f12-C2 (Δ*fig1*::*FIG1 MID1 CCH1*).

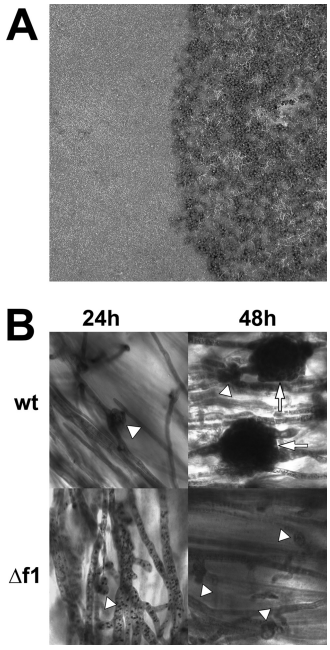

FIG 5 Sexual development of *F. graminearum* wt and Δfig1-1. (A) Mature wt culture (right) with normal sexual development and Δfig1-1 culture (left) with no perithecia. (B) Sexually induced cultures at 24 and 48 h stained with toluidine blue. Perithecium initials (arrowheads), which developed at 24 h in the wt, were barely initiated in Δfig1-1 cells. By 48 h, there were immature walled perithecia (arrow) in wt cells; in Δfig1-1 cells, perithecium initials have not matured and do not develop further. Scale bars, 20 μm. Abbreviations for strains and genotypes are listed in the legend of Fig. 3.

subsequent experiments. Two progeny, fig1a-22 and fig1a-23, lacked both *fig1* and the mating type *A*-2 gene.

To examine the effect of the loss of Fig1 on calcium homeostasis, YPD agar was inoculated with FGSG_4200 (wt mating type *a*), FGSG_2489 (wt mating type *A*), FGSC_17273 (Δ*fig1* mating type *a*), and fig1A-21 (Δ*fig1* mating type *A*), and the cultures were spot treated with the calcium ionophore A23187 or EtOH as a control. The cultures were examined at 38 h postinoculation, and all strains colonized the treated medium without any noticeable differences (data not shown). Crosses were initiated between the Δ*fig1* strains of both mating types to each other and to the opposite wt mating type strains to observe the effects of the loss of Fig1 on sexual development (Fig. 6). Development proceeded normally in all crosses, and mature perithecia formed, except for those in which *fig1* mating type *a* provided the protoperithecia. These *fig1* mating type *a* females, FGSC_17273, fig1a-22, and fig1a-23, failed to produce fertile perithecia following the addition of mating type *A* micro- and macroconidia. A microscopic examination of squashed perithecia showed that the fruiting bodies of the Δ*fig1* mating type *a* strain were not fertile, as they were devoid of asci and ascospores, but the Δ*fig1* mating type *A* strain developed normally (Fig. 7). A comparison of macroconidiation in wt mating type *a*, Δ*fig1* mating type *a*, and Δ*fig1* mating type *A* indicated no significant differences in conidiation among the strains.

DISCUSSION

The results presented here demonstrate divergent roles for Fig1 in *F. graminearum* and *N. crassa*. In *F. graminearum*, Fig1 function affects all stages of the life cycle examined and is essential for sexual development. In *N. crassa*, the loss of Fig1 resulted in little to no effect on vegetative growth but reduced female fertility and arrested perithecium development in a mating type *a* background. Fig1 is required for both Ca^{2+} influx-dependent and -independent responses to exposure to mating pheromone in yeasts (24, 43, 69, 73); however, to date, there have been no reported functional studies of Fig1 in filamentous species. The apparent divergence of LACS function between *N. crassa* and *F. graminearum* is reminiscent of the previously reported divergence of HACS function between *F. graminearum* and *N. crassa* in which both similar (slowed vegetative growth and calcium homeostasis lesions) and divergent (reduced ascospore discharge and abnormal ascospore morphology in *F. graminearum* and altered hyphal electrophysiology in *N. crassa*) phenotypes were observed (17, 40). The finding that the roles of the HACS and LACS both show divergence points to the evolutionary malleability of calcium signaling.

Recent studies, including an analysis of genomes in the Origins of Multicellularity Database (http://www.broadinstitute.org/annotation/genome/multicellularity_project/MultiHome.html), have suggested that some components of calcium

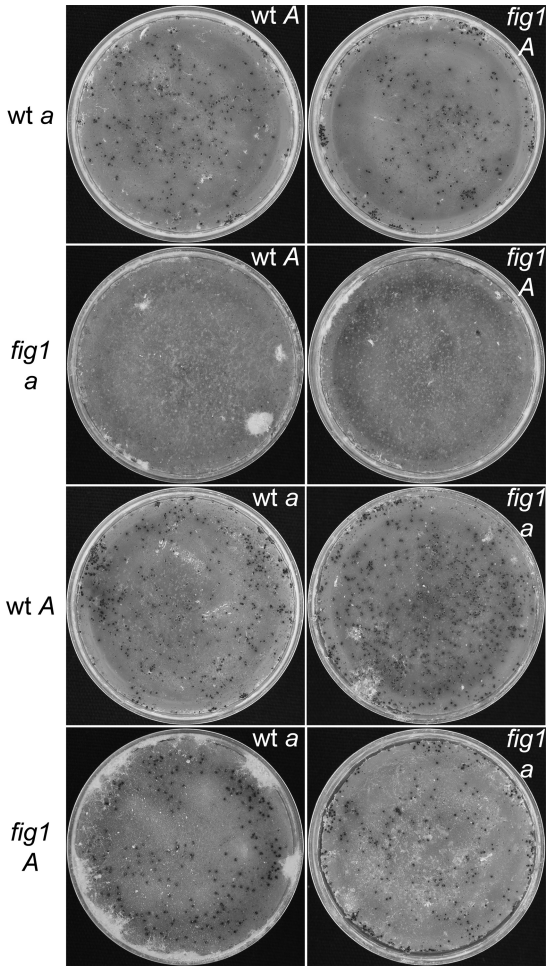

FIG 6 Reciprocal crosses of *N. crassa* wt and Δ*fig1* strains. Strains listed to the left served as females, developing protoperithecia that were fertilized by conidia of the strain listed in the upper right of each image. All crosses produced wt perithecia, except for crosses with Δ*fig1* mating type *a* strains as the female, which produced small infertile fruiting bodies. Abbreviations for strains are as follows: wt *a*, FGSC_4200; wt *A*, FGSC_2489; Δ*fig1 a*, FGSC_17273; Δ*fig1 A*, fig1A-18.

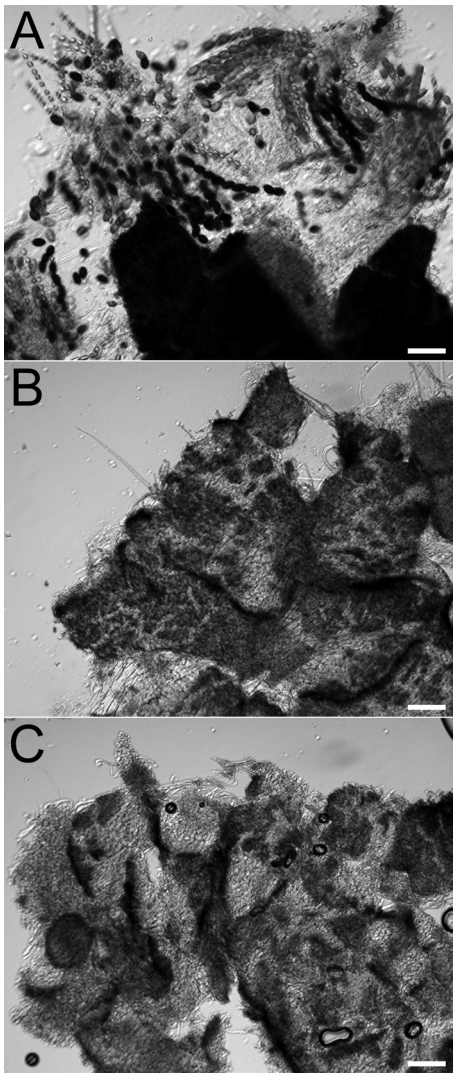

FIG 7 *N. crassa* perithecium squash mounts from wt and Δ*fig1* crosses. (A) Perithecium from a wt *a* × Δ*fig1 A* cross showing normal development, with asci and ascospores. (B) Infertile fruiting body from a Δ*fig1 a* × wt *A* cross. (C) Infertile fruiting body from a Δ*fig1 a* × Δ*fig1 A* cross. Scale bars, 75 μm. Abbreviations for strains are described in the legend of Fig. 6.

signaling once thought to be unique to either fungi or metazoans appeared before the divergence of these lineages approximately a billion years ago (10, 55, 57). The genome of *Thecamonas trahens*, a member of the phylum Apusozoa, was reported to contain the only known ortholog of Mid1 outside the true fungi. The Apusozoa are a possible sister group of the opisthokonts, having diverged before the fungal-metazoan split (15, 16, 31). However, BLASTP, BLASTX, and TBLASTN searches of the *T. trahens* genome or predicted proteins using the full-length Mid1 protein sequences from *F. graminearum* and *S. cerevisiae* and default settings failed to find a match. In addition, *T. trahens* contains several homologs of the mammalian VGCC rather than a fungal Cch1 ortholog. Furthermore, *Allomyces macrogynus*, a blastocladiomycete (39), possesses six Cch1 homologs (10). Although the presence of Fig1 and other PMP22_Claudin superfamily members was not examined by Cai and Clapman (10), multiple members are already known to exist in both metazoans and fungi, suggesting that at least one member was present in the common ancestor. Taken together, it appears that lineage-specific adaptation resulting in the loss, gain, or expansion of calcium signaling components in combination with the changes in specific roles may account for the differences seen in the extant species of unikont organisms.

Members of the PMP22_Claudin superfamily, of which Fig1 is a member, are involved in membrane-to-membrane interactions and also commonly form diffusion barriers that selectively allow ions, water, and other solutes to pass between cells (28, 33, 56, 68). The known functions of Fig1 in fungi fit well with those of non-fungal proteins in the PMP22_Claudin superfamily, involving cell-to-cell interactions and ion flux. Fig1 is involved in the sexual development of *C. albicans* and *S. cerevisiae*, and the results here show that it is also involved in the sexual development of *F. graminearum* and *N. crassa*. *Fig1* expression and calcium uptake increase in response to mating pheromone, and Fig1 localizes to the mating projections and membranes destined for fusion during mating in both *S. cerevisiae* and *C. albicans*. The deletion of *FIG1*

resulted in lowered pheromone-induced calcium accumulation and decreased cell fusion during the mating of both yeasts. For *S. cerevisiae*, undigested cell wall remaining between the appressed shmoos was observed, which was rescued by the addition of exogenous calcium, and this phenotype was not seen for *C. albicans* (2, 24). Cell-to-cell interactions and membrane dynamics appear to be central to the function of Fig1 in yeast mating and point to a possible similar role in filamentous fungi that may explain the blocking of sexual development in *F. graminearum* and the reduced female fertility of *N. crassa* seen for Δ*fig1* mutants. Cellular fusion is critical to the formation of the coiled perithecium initials and the formation of parenchymatous tissue from hyphae during fruiting (61). Although the blocking of *F. graminearum* sexual development did not allow an investigation of the role of Fig1 in later stages of development in the present study, expression data suggest that Fig1 is involved at later stages of *F. graminearum* sexual development. Membrane dynamics and trafficking are essential for ascus development (3, 37, 54) and for the delimitation of ascospores by the formation of double membranes around the progeny nuclei (21, 67). As Fig1 is involved in membrane fusion, a role for Fig1 in ascus development and ascospore delimitation is possible.

The mating-type-specific defect of *N. crassa* Δ*fig1* mating type *a* strains, while different from the *F. graminearum* results, is reminiscent of the results seen for yeasts. For *S. cerevisiae*, Fig1 expression was triggered in *MAT***a** cells upon exposure to α-pheromone, and although expression in *MAT*α cells was not reported, some mating defects were more severe in Δ*fig1* × Δ*fig1* crosses than in Δ*fig1* × wt (*MAT*α) crosses (24), suggesting at least some *FIG1* expression in *MAT*α strains. In *C. albicans*, *CaFIG1* expression occurs only in opaque-phase cells homozygous for mating type locus *a* (*MTLa*) upon exposure to α-pheromone and not in *MTL* heterozygotes or *MTL*α homozygotes (43). While the details are slightly different, the commonality is that Fig1 plays a greater role in one mating type, the *a* idiomorph, than in the other. In contrast to these systems, *F. graminearum* is homothallic and effectively always contains both mating types, which may have eliminated the mating type constraints on Fig1 expression and, possibly, function.

The role of Fig1 in vegetative growth is also variable among the fungi. The loss of Fig1 did not affect the growth rate or calcium accumulation of *S. cerevisiae* or *C. albicans* vegetative yeast cells (9, 49). During the hyphal growth of *C. albicans*, the *CaFIG1* expression level was low, and fluorescence from CaFig1-green fluorescent protein (GFP) fusion proteins was undetectable but was increased upon exposure to mating pheromone (70). The deletion of *CaFIG1* resulted in an increased conversion to hyphal growth of yeast cells grown on agar, indicating that CaFig1 plays a role in hyphal suppression in some environments (9). Additionally, the loss of CaFig1 did not decrease calcium uptake in *C. albicans* hyphae but did affect the thigmotropic response of hyphae to physical ridges, resulting in a reduced frequency of hyphal tip growth reorientation upon contact with a ridge compared to the wt (9). Our results show that the loss of *fig1* had no detectable effect on *N. crassa* vegetative growth. However, in *F. graminearum*, the *FIG1* deletion resulted in phenotypes similar to those for HACS mutants: reduced vegetative growth, reduced macroconidiation, and defective calcium homeostasis (17, 35). The mycelium of HACS mutants was fluffy compared to that of the wt, while mycelia of Δ*fig1* strains were appressed to the substrate surface, with few aerial hyphae. The nutrient availability seemed to affect this phenotype, as fewer aerial hyphae were produced on V8 agar than on the more-nutrient-rich carrot agar. Another difference is that the Δ*fig1* mutants and the wt grew on calcium-limited medium supplemented with BAPTA, but Δ*mid1* and Δ*cch1* strains failed to colonize the BAPTA-containing medium, suggesting the need for the HACS, but not the LACS, to support calcium influx in calcium-limited environments. It would be interesting to see if the LACS has a function in the hyphal electrophysiology of *F. graminearum* and *N. crassa*. A disruption of the HACS in *N. crassa* resulted in altered electrical properties, as measured by a voltage clamp (40). In contrast, a disruption of the HACS in *F. graminearum* did not alter the hyphal electrochemical properties (17).

The results presented here, taken together with the results of previous studies of the HACS and LACS in fungi and the analysis of calcium signaling components in the Origins of Multicellularity Database, show the evolutionary flexibility of calcium signaling in the different lineages of extant eukaryotes. Even within the Sordariomycetes, the roles of the HACS and LACS have diverged, as suggested by studies of Cch1, Mid1, and Fig1 of *F. graminearum* and *N. crassa*. Although not examined here because of the block in sexual development, it is likely that Fig1 plays a role in sexual development after the transition from perithecium initials to the immature perithecium, and the application of sexual development stage specific or inducible RNA interference (RNAi) would allow the investigation of any such role. Additionally, the documented roles of calcium importation genes in sexual development suggest that other calcium signaling components will also be involved. Finally, the end targets of calcium signaling during sexual development are not known, and investigations to identify them are in progress.

ACKNOWLEDGMENTS

We thank the Fungal Genetics Stock Center, which provided the *Neurospora* strains used in this study. We thank Nick Harrison for technical assistance.

We acknowledge the support of the National Science Foundation (grant 0923794 to F.T.) and Michigan AgBioResearch.

REFERENCES

1. **Abràmoff MD, Magalhães PJ, Ram SJ.** 2004. Image processing with ImageJ. Biophotonics Int. **11**:36–42.
2. **Alby K, Schaefer D, Sherwood RK, Jones SK, Jr, Bennett RJ.** 2010. Identification of a cell death pathway in *Candida albicans* during the response to pheromone. Eukaryot. Cell **9**:1690–1701.
3. **Beckett A, Crawford RM.** 1973. The development and fine structure of the ascus apex and its role during spore discharge in *Xylaria longipes*. New Phytol. **72**:357–369.
4. **Berridge MJ, Bootman MD, Roderick HL.** 2003. Calcium signalling: dynamics, homeostasis and remodelling. Nat. Rev. Mol. Cell Biol. **4**:517–529.
5. **Booth C.** 1971. The genus *Fusarium*. Commonwealth Mycological Institute, Kew, Surrey, England.
6. **Bormann J, Tudzynski P.** 2009. Deletion of Mid1, a putative stretch-activated calcium channel in *Claviceps purpurea*, affects vegetative growth cell wall synthesis and virulence. Microbiology **155**:3922–3933.
7. **Bowden RL, Leslie JF.** 1999. Sexual recombination in *Gibberella zeae*. Phytopathology **89**:182–188.
8. **Brand A, Lee K, Veses V, Gow N.** 2009. Calcium homeostasis is required for contact-dependent helical and sinusoidal tip growth in *Candida albicans* hyphae. Mol. Microbiol. **71**:1155–1164.
9. **Brand A, et al.** 2007. Hyphal orientation of *Candida albicans* is regulated by a calcium-dependent mechanism. Curr. Biol. **17**:347–352.
10. **Cai X, Clapman DE.** 2012. Ancestral Ca^{2+} signaling machinery in early animal and fungal evolution. Mol. Biol. Evol. **29**:91–100.

11. **Camacho C, et al.** 2009. BLAST+: architecture and applications. BMC Bioinformatics **10**:421–429.
12. **Cappellini RA, Peterson JL.** 1965. Macroconidium formation in submerged cultures by a non-sporulating strain of *Gibberella zeae*. Mycologia **57**:962–966.
13. **Carroll AM, Sweigard JA, Valent B.** 1994. Improved vectors for selecting resistance to hygromycin. Fungal Genet. Newsl. **41**:22.
14. **Catlett NL, Lee B, Yoder OC, Turgeon BG.** 2003. Split-marker recombination for efficient targeted deletion of fungal genes. Fungal Genet. Newsl. **50**:9–11.
15. **Cavalier-Smith T.** 2009. Megaphylogeny, cell body plans, adaptive zones: causes and timing of eukaryote basal radiations. J. Eukaryot. Microbiol. **56**:26–33.
16. **Cavalier-Smith T, Chao EE.** 2010. Phylogeny and evolution of Apusomonadida (Protozoa: Apusozoa): new genera and species. Protist **161**: 549–576.
17. **Cavinder B, Haman A, Lew RR, Trail F.** 2011. Mid1, a mechanosensitive calcium ion channel, affects growth, development, and ascospore discharge in the filamentous fungus *Gibberella zeae*. Eukaryot. Cell **10**:832–841.
18. **Cock PJA, et al.** 2009. Biopython: freely available Python tools for computational molecular biology and bioinformatics. Bioinformatics **25**: 1422–1423.
19. **Colot HV, et al.** 2006. A high-throughput gene knockout procedure for *Neurospora* reveals functions for multiple transcription factors. Proc. Natl. Acad. Sci. U. S. A. **103**:10352–10357.
20. **Courchesne WE, Vlasek C, Klukovich R, Coffee S.** 2011. Ethanol induces calcium influx via the Cch1-Mid1 transporter in *Saccharomyces cerevisiae*. Arch. Microbiol. **193**:323–334.
21. **Czymmek KJ, Klomparens KL.** 1992. The ultrastructure of ascosporogenesis in freeze-substituted *Thelebolus crustaceus*: enveloping membrane system and ascospore initial development. Can. J. Bot. **70**:1669–1683.
22. **Davis RL, de Serres D.** 1970. Genetic and microbial research techniques for *Neurospora crassa*. Methods Enzymol. **27A**:79–143.
23. **Di Tommasao P, et al.** 2011. T-Coffee: a Web server for the multiple sequence alignment of protein and RNA sequences using structural information and homology extension. Nucleic Acids Res. **39**:W13–W17. doi: 10.1093/nar/gkr245.
24. **Erdman SE, Lin L, Malczynski M, Snyder M.** 1998. Pheromone regulated genes required for yeast mating differentiation. J. Cell Biol. **140**:461–483.
25. **Fairhead C, Thierry A, Denis F, Eck M, Dujon B.** 1998. 'Mass-murder' of ORFs from three regions of chromosome XI from *Saccharomyces cerevisiae*. Gene **223**:33–46.
26. **Fairhead C, Llorente B, Denis F, Soler M, Dujon B.** 1996. New vectors for combinatorial deletions in yeast chromosomes and for gap-repair cloning using 'split-marker' recombination. Yeast **12**:1439–1457.
27. **Fischer M, et al.** 1997. The *Saccharomyces cerevisiae* CCH1 gene is involved in calcium influx and mating. FEBS Lett. **419**:259–262.
28. **Furuse M.** 2010. Claudins, tight junctions, and the paracellular barrier. Curr. Top. Membr. **65**:1–19.
29. **Gaffoor I, et al.** 2005. Analysis of the polyketide synthase genes in the filamentous fungus *Gibberella zeae* (anamorph *Fusarium graminearum*). Eukaryot. Cell **4**:1926–1933.
30. **Glass NL, et al.** 1988. DNAs of the two mating-type alleles of *Neurospora crassa* are highly dissimilar. Science **241**:570–573.
31. **Glücksman E, et al.** 2011. The novel marine gliding zooflagellate genus *Mantamonas* (Mantamonadida ord. n.: Apusozoa). Protist **162**:207–221.
32. **Gouy M, Guindon S, Gascuel O.** 2010. SeaView version 4: a multiplatform graphical user interface for sequence alignment and phylogenetic tree building. Mol. Biol. Evol. **27**:221–224.
33. **Grey AC, Jacobs MD, Gonen T, Kistler J, Donaldson PJ.** 2003. Insertion of MP20 into lens fibre cell plasma membranes correlates with the formation of an extracellular diffusion barrier. Exp. Eye Res. **77**:567–574.
34. **Groppi S, Belotti F, Brandão RL, Martegania E, Tisi R.** 2011. Glucose-induced calcium influx in budding yeast involves a novel calcium transport system and can activate calcineurin. Cell Calcium **49**:376–386.
35. **Hallen H, Trail F.** 2008. The L-type calcium ion channel Cch1 affects ascospore discharge and mycelial growth in the filamentous fungus *Gibberella zeae* (anamorph *Fusarium graminearum*). Eukaryot. Cell **7**:415–424.
36. **Hong MP, Vu K, Bautos J, Gelli A.** 2010. Cch1 restores intracellular Ca^{2+} in fungal cells during ER stress. J. Biol. Chem. **285**:10951–10958.
37. **Hung CY, Wells K.** 1977. The behavior of the nucleolus during nuclear divisions in the asci of *Pyronema domesticum*. Mycologia **69**:685–692.
38. **Iida H, Nakamura H, Ono T, Okumura M, Anraku Y.** 1994. MID1, a novel *Saccharomyces cerevisiae* gene encoding a plasma membrane protein, is required for Ca^{2+} influx and mating. Mol. Cell. Biol. **14**:8259–8271.
39. **James TY, et al.** 2006. A molecular phylogeny of the flagellated fungi (Chytridiomycota) and description of a new phylum (Blastocladiomycota). Mycologia **98**:860–871.
40. **Lew RR, Abbas Z, Anderca M, Free S.** 2008. Phenotype of a mechanosensitive channel mutant, *mid-1*, in a filamentous fungus, *Neurospora crassa*. Eukaryot. Cell **7**:647–655.
41. **Li H, Durbin R.** 2009. Fast and accurate short read alignment with Burrows-Wheeler Transform. Bioinformatics **25**:1754–1760.
42. **Locke E, Bonilla M, Liang L, Takita Y, Cunningham K.** 2000. A homolog of voltage-gated Ca^{2+} channels stimulated by depletion of secretory Ca^{2+} in yeast. Mol. Cell. Biol. **20**:6686–6694.
43. **Lockhart SR, et al.** 2002. In *Candida albicans*, white-opaque switchers are homozygous for mating type. Genetics **162**:737–745.
44. **Marchler-Bauer A, et al.** 2011. CDD: a conserved domain database for the functional annotation of proteins. Nucleic Acids Res. **39**:D225–D229. doi: 10.1093/nar/gkq1189.
45. **Martin DC, et al.** 2011. New regulators of a high affinity Ca^{2+} influx system revealed through a genome-wide screen in yeast. J. Biol. Chem. **286**:10744–10754.
46. **Matter K, Balda MS.** 2003. Signalling to and from tight junctions. Nat. Rev. Mol. Cell. Biol. **4**:225–237.
47. **Metzenberg RL, Glass NL.** 1990. Mating type and mating strategies in Neurospora. Bioessays **12**:53–59.
48. **Michalak M, Parker JMR, Opas M.** 2002. Ca^{2+} signaling and calcium binding chaperones of the endoplasmic reticulum. Cell Calcium **32**:269–278.
49. **Muller E, Mackin N, Erdman S, Cunningham K.** 2003. Fig1p facilitates Ca^{2+} influx and cell fusion during mating of *Saccharomyces cerevisiae*. J. Biol. Chem. **278**:38461–38469.
50. **Paidhungat M, Garrett S.** 1997. A homolog of mammalian, voltage-gated calcium channels mediates yeast pheromone-stimulated Ca^{2+} uptake and exacerbates the cdc1(Ts) growth defect. Mol. Cell. Biol. **17**:6339–6347.
51. **Peiter E, Fischer M, Sidaway K, Roberts S, Sanders D.** 2005. The *Saccharomyces cerevisiae* Ca^{2+} channel Cch1pMid1p is essential for tolerance to cold stress and iron toxicity. FEBS Lett. **579**:5697–5703.
52. **Perkins DD.** 2006. How to convert wild-type spreading growth to colonial. Fungal Genetics Stock Center, Kansas City, MO. http://www.fgsc.net/neurospora/NeurosporaProtocolGuide.htm. Accessed March 2011.
53. **R Development Core Team.** 2010. R: a language and environment for statistical computing. R Foundation for Statistical Computing, Vienna, Austria. http://www.R-project.org/.
54. **Read ND, Beckett A.** 1996. Ascus and ascospore morphogenesis. Mycol. Res. **100**:1281–1314.
55. **Rokas A.** 2008. The origins of multicellularity and the early history of the genetic toolkit for animal development. Annu. Rev. Genet. **42**:235–251.
56. **Rosenthal R, et al.** 2010. Claudin-2, a component of the tight junction, forms a paracellular water channel. J. Cell Sci. **129**:1919–1921.
57. **Ruiz-Trillo I, Roger AJ, Burger G, Gray MW, Lang BF.** 2008. A phylogenomic investigation into the origin of metazoa. Mol. Biol. Evol. **25**: 664–672.
58. **Shear CL, Dodge BO.** 1927. Life histories and heterothallism of the red bread-mold fungi of the *Monilia sitophila* group. J. Agric. Res. **34**:1019–1042.

58a. **Sikhakolli UR, et al.** 14 June 2012, posting date. Transcriptome analyses during fruiting body formation in *Fusarium graminearum* and *Fusarium verticillioides* reflect species life history and ecology. Fungal Genet. Biol. doi:10.1016/j.fgb.2012.05.009.

59. **Strickland WN, Perkins DD.** 1973. Rehydrating ascospores to improve germination. Neurospora Newsl. **20**:34–35.
60. **Thom C, Church MB.** 1926. The aspergilli. Williams & Wilkins Co, Baltimore, MD.
61. **Trail F, Common R.** 2000. Perithecial development by *Gibberella zeae*: a light microscopy study. Mycologia **92**:130–138.
62. **Trail F, Xu H, Loranger R, Gadoury D.** 2002. Physiological and environmental aspects of ascospore discharge in *Gibberella zeae* (anamorph *Fusarium graminearum*). Mycologia **94**:181–189.
63. **Trail F, Gaffoor I, Vogel S.** 2005. Ejection mechanics and trajectory of the

ascospores of *Gibberella zeae* (anamorph *Fusarium graminearum*). Fungal Genet. Biol. **42**:528–533.
64. **Tsukita S, Furuse M, Itoh M.** 1999. Structural and signalling molecules come together at tight junctions. Curr. Opin. Cell Biol. **11**:628–633.
65. **Viladevall L, et al.** 2004. Characterization of the calcium-mediated response to alkaline stress in *Saccharomyces cerevisiae*. J. Biol. Chem. **279**: 43614–43624.
66. **Waterhouse AM, Procter JB, Martin DM, Clamp M, Barton GJ.** 2009. Jalview version 2—a multiple sequence alignment editor and analysis workbench. Bioinfomatics. **25**:1189–1191.
67. **Wu CG, Kimbrough JW.** 2001. Ascosporogenesis in *Tarzetta* (Otideaceae, Pezizales). Int. J. Plant Sci. **162**:1075–1080.
68. **Wu TS, Linz JE.** 1993. Recombinational inactivation of the gene encoding nitrate reductase in *Aspergillus parasiticus*. Appl. Environ. Microbiol. **59**: 2998–3002.
69. **Wu VM, Schulte J, Hirschi A, Tepass U, Beitel GJ.** 2004. Sinuous is a Drosophila claudin required for septate junction organization and epithelial tube size control. J. Cell Biol. **164**:313–323.
70. **Yang M, et al.** 2011. Fig1 facilitates calcium influx and localizes to membranes destined to undergo fusion during mating in *Candida albicans*. Eukaryot. Cell **10**:435–444.
71. **Zerbino DR, Birney E.** 2008. Velvet: algorithms for de novo short read assembly using de Bruijn graphs. Genome Res. **18**:821–829.
72. **Zerbino DR, McEwen GK, Margulies EH, Birney E.** 2009. Pebble and rock band: heuristic resolution of repeats and scaffolding in the Velvet short-read *de novo* assembler. PLoS One **4**:e8407. doi:10.1371/journal.pone.0008407.
73. **Zhang NN, et al.** 2006. Multiple signaling pathways regulate yeast cell death during the response to mating pheromones. Mol. Biol. Cell **17**: 3409–3422.